The International Society for Optical Engineering

To download the electronic version of this newsletter, please go to:
http://spie.org/membership/ei/pdfs/ei15-2.pdf

JUNE 2005
VOL. 15, NO. 2

ELECTRONIC IMAGING

Newsletter of the SPIE Electronic Imaging Technical Group

***Gabriel Marcu,** Apple Computer, Inc.*
Editor/Technical Group Chair

Contents

Imaging arithmetic: Physics ∪ Math > Physics + Math

Gaurav Sharma, Electrical and Computer Engineering and Biostatistics & Computational Biology Depts., University of Rochester

For several real-world problems, the mathematical methods of signal and image processing are most successful when they also incorporate the insight offered by the physics of the problem. Imaging systems are a particularly fertile ground for problems in this class because they deal specifically with the capture of physical scenes and with the reproduction of images on physical devices. Solutions for these problems that combine physical understanding and modeling with appropriate mathematical tools of signal/image processing, offer advantages significantly greater than the sum of the individual parts. In this article, we illustrate how the happy marriage between physical insight and modeling and appropriate mathematical methods leads to novel solutions. Additional examples and references may be found in the identically-titled paper presented at the January 2005 IS&T/SPIE Electronic Imaging meeting.[1]

Show-through in document imaging

Duplex or double-sided printing is commonly used for hardcopy documents, with most magazine and book pages being prime examples. When a duplex-printed page is scanned, infor-

Continued on page 10.

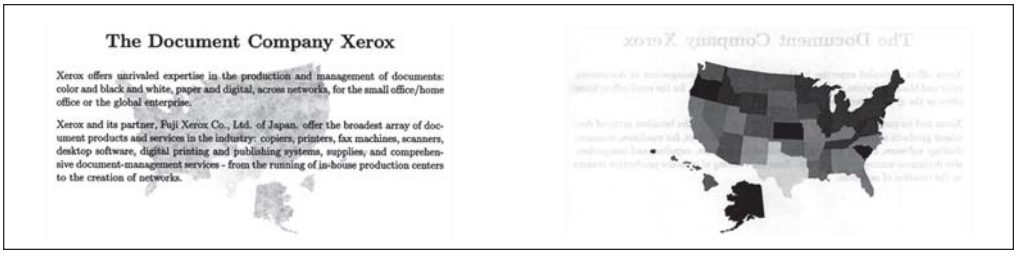

Figure 1. Scans of two sides of a duplex-printed page.[3]

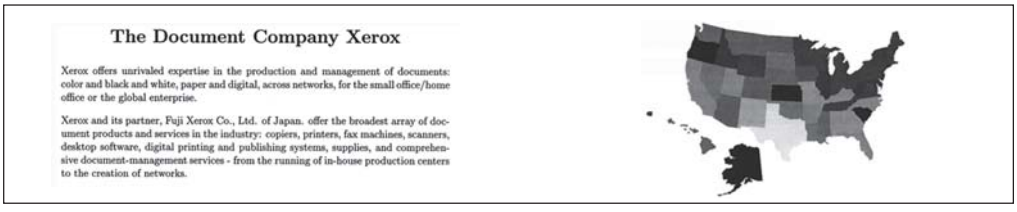

Figure 2. Scanned data after show-through correction.[3]

A simple optical system for real-time size measurements of nuclear fuel pellets

Thomas P. Karnowski, Andrew K. Kercher, John D. Hunn, and L. Curt Maxey, Oak Ridge National Laboratory

Advanced nuclear reactor designs use fuel forms that are built up from tens of thousands of tiny nuclear fuel pellets. Called TRISO (tri-isotropic) particles, these employ a dense layer of silicon carbide to trap radioactive fission products. The coated TRISO fuel acts as a containment system to prevent the release of fission products to the environment during accidents. Furthermore, these advanced nuclear reactor designs are regarded as an important part of the future hydrogen economy because they can be used to produce hydrogen more efficiently than electrolysis.[1] Rapid counting and measurement of TRISO spheres is a necessary technology for the development of these materials. A survey of commercial equipment found available devices lacking in speed, resolution, and accuracy. We therefore elected to develop this capability in-house.

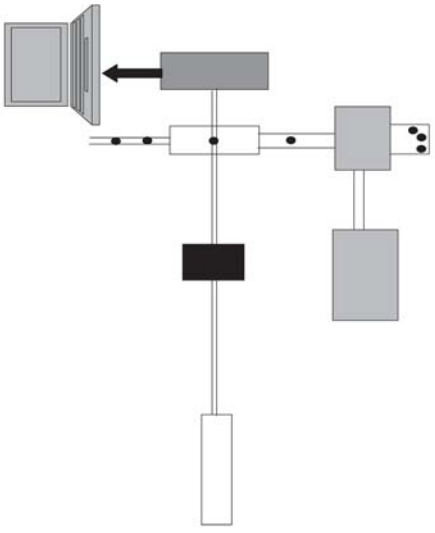

Figure 1. Schematic of the optical system. Particles are carried by vacuum pump through a target cell where they are illuminated by a laser line. The resultant blocked signal is detected and processed by the computer.

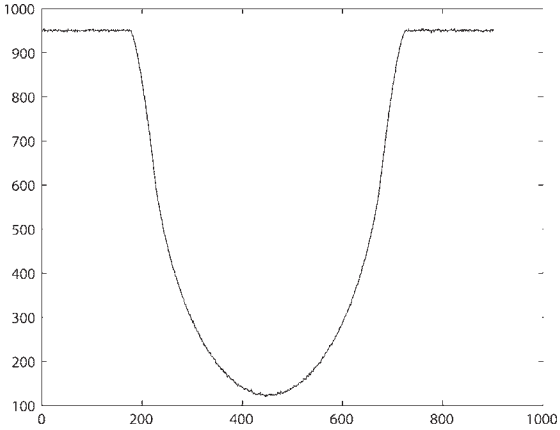

Figure 2. A typical event where a particle passes through the laser line and is detected. The shape is similar to a parabola.

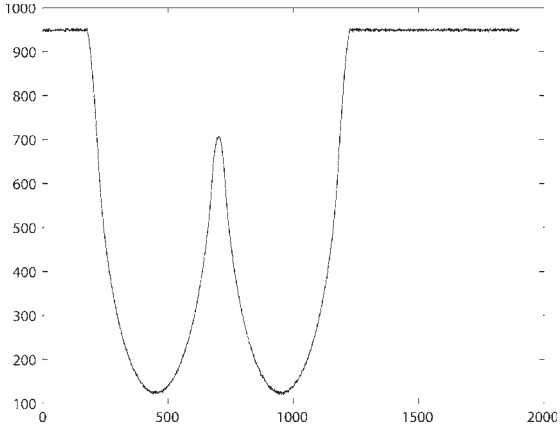

Figure 3. An abnormal event where multiple particles pass through the laser line. This shape deviates considerably from a parabola and can be detected as an abnormal event for later manual inspection.

Based on the methods used by Wallisch and Koss[2] we employed a light obstruction concept where a slit of light (either an aperture or a focused beam) is blocked by a particle. The system projects light through a target transport cell and collects the light onto a photo receiver (see Figure 1). The signal from this receiver is digitized by a high-speed analog-to-digital conversion unit (ADC), and is shown in Figure 2. When no light is blocked, the signal is high, but it then shrinks as the sphere passes through the slit and reaches a minimum when the sphere blocks the maximum amount of light. The maximum light blockage is proportional to the diameter of the sphere.

The error in our measurement can be limited by the ADC resolution since we are trying to estimate the radius with the intensity of the obstruction. We attempt to better estimate the peak location by fitting the data to a parabola. In our software this is accomplished by finding the sampled peak, then locating 80 values on either side of it. These 161 values are used to find the coefficients of a least-squares error fit to a parabola, and to estimate the 'true' minimum value of the curve. This improves the accuracy of the ADC resolution by a factor of 100.

Another problem was linked to the size of the particle-handling system, which was designed for 1000μm spheres. When smaller spheres (800μm) pass through the cell, some overlapping can occur, causing a signal that deviates significantly from the ideal event (see Figure 3). We detect these in real-time by determining the error between the event and a three-point parabolic fit. Large errors indicate several particles may have been detected together. This provides an easy-to-compute method for finding multi-particle events that can be manually screened with software tools.

Experiments have estimated the counting accuracy as having an error of less than 0.075% with a 95% confidence. The size-measurement accuracy was on the order of 11μm standard deviation for spheres 1000μm in diameter. Although the current particle transport system does not support the maximum detection rate, electronically-generated data showed rates of 200 particles per second, implying a throughput of 720,000 particles per hour. These rates and accuracies will improve the research and development cycle for the manufacturing of these pellets: which will ultimately lead to safer, more-efficient nuclear reactors producing energy to benefit us all.

Thomas P. Karnowski,
Andrew K. Kercher, John D. Hunn,
and L. Curt Maxey
Oak Ridge National Laboratory, TN

References

1. **ORNL Review 35** (2), 2002.
2. K. Wallisch and P. Koss, *Automatic size analysis of coated fuel particles,* **Nucl. Tech. 35**, pp. 279-283, 1977.

Machine vision for defect detection on silicon wafers

Fabrice Meriaudeau, Patrick Gorria, Le2i Laboratory, University of Burgundy; **Pierrick Bourgeat,** BioMedIA Laboratory, CSIRO; **Kenneth Tobin,** Oak Ridge National Laboratory

Silicon wafers are extensively used in the semiconductor and microelectronics industries. With this material, it is of extreme importance to obtain a defect-free surface to improve yield and microchip performance. Current practice in the industry is to inspect the wafers for surface defects only at the end of the final polishing stage. Techniques such as atomic force microscopy, scanning tunneling force microscopy, scanning electron microscopy, x-rays and acoustic electron microscopy have all been used to perform the surface-defect characterization. However, all these methods require cumbersome equipment that is expensive to use on a daily basis in a production factory.

We have developed an alternative technique that relies on the use on the direct-to-digital holography (DDH).[1] This allows us to capture the complex image of a scene, and then reconstruct the phase and amplitude information. This gives us a complete 3D representation of the scene within the wavelength depth of the laser used to produce the hologram: thus it provides a new dimension to texture analysis.[2,3]

In die-to-die wafer inspection (see Figure 1), defect detection is based on the comparison of the same area on two neighboring dies. Images being thoroughly aligned, the dissimilarities between the images are a result of defects in the area of one of the dies. The two images are subtracted, and a threshold level is selected to locate any anomaly.

To optimize the signal-to-noise ratio, the threshold value is established based upon the noise level in the difference image. However, since multiple structures coexist in the same field of view, the noise level can vary over a single image preventing the use of a global threshold. To overcome this problem, a segmentation is done to create a mask of the different regions (each region being a class for our classifier) in order to produce a measure of noise for each structure in the difference image. This leads to an individual threshold for each region (see Figure 1).

The mask is created through a 'classification-segmentation' procedure. The complex image provided by the DDH is first processed to generate four new images: the phase, normalized-amplitude, and complex images; and also the complex image with normalized amplitude.[5] Each image is then processed using a bank of Gabor filters (see Figure 2), and then used as input in a vote SVM (support vector machine) classifier.[6]

A pixel is classified as pertaining to a given class (dynamic RAM, logic area, or blank area) if it is identified as such by at least two of the three best classifiers. A so-far unclassified pixel —a pixel identified as being part of a different class by each of these three classifiers—is identified according to the results of the fourth. Figure 3 shows an example of a segmented image. The obtained results show robust segmentation.[4,6]

The technique we developed enables us to train the classifier with a small set of examples and to obtain results similar to those produced using a full training set. The technique can be applied to any type of optical tool for wafer inspection, but in the particular case of the DDH, the extra information provided by the complex nature of the image, makes it even more powerful. The classification has been applied to defect detection and has led to a tremendous improvement in the final results:[4] the ratio of false detection to no detection.

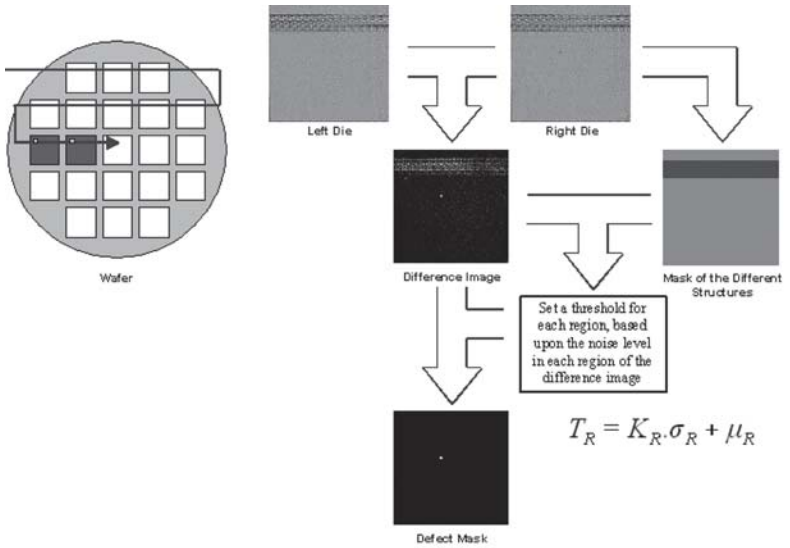

Figure 1. Principle of die-to-die wafer inspection and defect detection with the creation of a mask for local noise and threshold estimation. Respectively, μ and σ are the average grey and the standard deviation in the different regions.

Fabrice Meriaudeau, Pierrick Bourgeat*, Patrick Gorria, and Kenneth Tobin†
Le2i Laboratory
University of Burgundy, France
*BioMedIA Laboratory
CSIRO, Australia
†Oak Ridge National Laboratory, TN
E-mail: f.meriaudeau@iutlecreusot.u-bourgogne.fr

Continued on page 7.

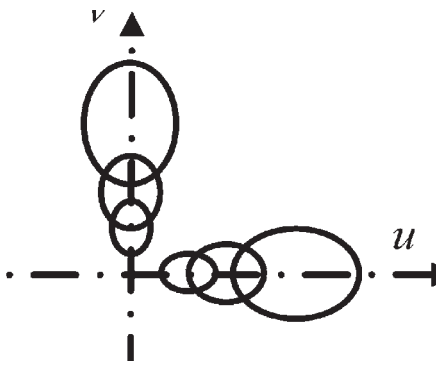

Figure 2. Bank of Gabor filters with three scales and two orientations.

Figure 3. Example of a segmented image.

Three-dimensional inspection of highly-reflective metallic objects by polarization imaging

Olivier Morel, Christophe Stolz, Fabrice Meriaudeau, and Patrick Gorria, Laboratory Le2i

In the field of industrial vision, 3D (three-dimensional) inspection of highly-reflective metallic objects is still a difficult task. Indeed, highlights prevent the use of a 3D laser scanner, and phase-shifting-based 3D systems are better adapted to the inspection of surfaces with low curvature. The 'shape from polarization' technique[1,2] can be extended to provide 3D information on highly-reflective metallic surfaces. After being reflected from an object, unpolarized light becomes partially-linearly polarized: to what extent and in what direction depends on the surface normal and the refractive index of the surface medium.[3] Once the surface normals are computed, the surface profile can be obtained by integration.

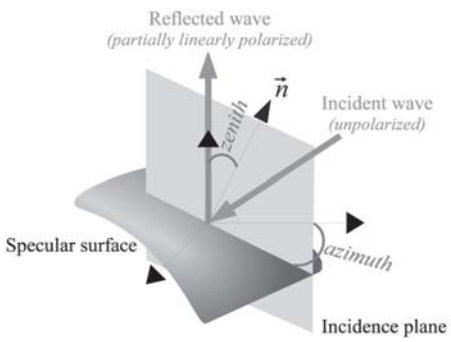

Figure 1. Reflection of a light wave from a highly-reflective surface.

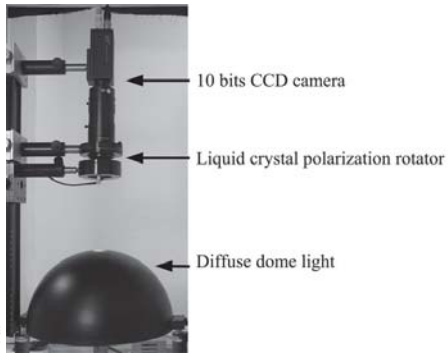

Figure 2. System to acquire the polarization of the reflected beam.

Partially-linearly-polarized light has three parameters: the intensity, and the angle and degree of polarization. The latter gives the proportion of the linearly-polarized component. For characterization, we can use a rotating polarizing filter in front of the camera. The relationship between the intensity and the rotation angle of the filter is given by a sinusoid. The phase shift gives the angle of polarization, and the degree of polarization is the relative magnitude of the sinusoid. To speed up the sensing of polarization components, the filter is replaced with an electrically-controlled liquid-crystal polarization rotator.

The polarization parameters of the reflected light are linked to the normals of the surface. On the one hand, the linearly-polarized component is orthogonal to the incidence plane, meaning that the angle of polarization gives the azimuth angle. On the other hand, by using the complex refractive index of the surface, and thanks to the Fresnel coefficients, a new relation between the degree of polarization and the zenith angle can be found.[4] Therefore, these two angles determine the surface normals (see Figure 1). The surface is then reconstructed from the normals by integration.

The acquisition system consists of a CCD camera, the liquid-crystal polarization rotator, and a diffuse dome light (see Figure 2) to supply unpolarized light across the whole surface. After being reflected, the light—which becomes partially-linearly polarized—is analyzed. Since the degree of polarization is lower for metallic surfaces, a sensitive camera with 10bit depth is used. In total, 18 frames are acquired with different polarization rotations from 0° to 180°, with a constant step of 10°. The least-mean-square method is applied during the acquisition process to compute the polarization parameters. Then, by knowing the object's complex index of refraction, the normals are computed and finally the surface is reconstructed by integration.

Figure 3. Polarization imaging applied to the 3D reconstruction of highly-reflective metallic objects: (a) object of reference photograph, (b) 3D reconstructed surface.

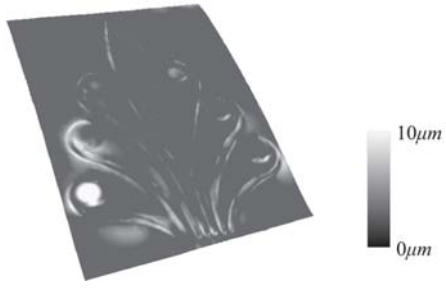

Figure 4. Mean deviation map between a flawless surface and a surface with a shape defect.

Results

Because of the manufacturing process, metallic objects made through stamping and polishing do not all come out the same way: thus 3D information has to be extracted in order to characterize them.

To compare the 3D surface obtained with our polarization system to a reference 3D surface, an object was coated with a thin opaque layer and scanned with a 3D commercial scanner (Replica 500). After registration of the two surfaces, the mean deviation between the surfaces was about 30μm. The reconstructed surface is presented on Figure 3. The resolution along the X and Y axes depend only on the lenses used and on the spatial resolution of the sensor: so X/Y resolutions of up to three times this accuracy should be achievable.

Figure 4 shows the comparison of a reconstructed surface from a flawless object and a defective part which has a shape defect (bump) on the left-bottom .

Conclusion

Polarization imaging presents a new way of reconstructing the 3D surface of highly-reflective metallic objects. The acquisition equipment—diffuse dome light, CCD camera, and liquid crystal polarization rotator—are quite simple. The system is fully automated, from the acquisition of the polarization parameters to the 3D surface reconstruction process. Further, it can be integrated with production lines to detect shape defects on objects made via stamping and polishing.

Continued on page xx.

Making 3D binary digital images well composed

Marcelo Siqueira, Jean Gallier, Department of Computer and Information Science, University of Pennsylvania; **Longin Jan Latecki,** Department of Computer and Information Sciences, Temple University

A three-dimensional binary digital image is said to be well composed if, and only if, the set of points in the voxel faces consisting of every voxel face that is shared by a foreground and a background voxel of the image is a 2D manifold.[1] A well-composed image enjoys very useful topological and geometric properties. These properties make simpler several basic algorithms in computer vision, computer graphics, and image processing. For instance, thinning algorithms do not suffer from the irreducible thickness problem if the image is well composed.[2] Also, algorithms that rely on curvature computation to extract approximating iso-surfaces directly from binary images can be applied to well-composed images with no need to handle special cases resulting from 'non-manifold' topology.[3,4]

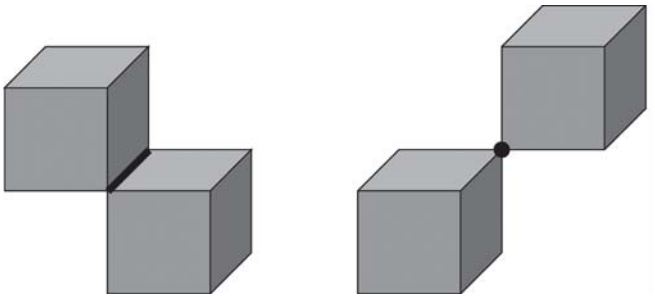

Figure 1. Instances of the two critical configurations. For the sake of clarity, only the background voxels are shown. The shared edge (left) of the first critical configuration and the shared vertex (right) of the second are heavily drawn.

On the other hand, if a 3D digital binary image is the result of the digitization of a 'solid' object, such as a bone, and it lacks the property of being well composed. In this case, the digitization process that gave rise to it is not topology-preserving. As the results in Reference 5 show, if the resolution of the digitization process is fine enough to ensure preservation of topology, then the resulting image is well composed. This fact has motivated us to develop an iterative and randomized algorithm for 'repairing' non well-composed 3D digital binary images.

Our algorithm restores the given image by converting background voxels into foreground ones. Although this algorithm always produces a well-composed image, it cannot guarantee that the result is the same as would be obtained from a topology-preserving digitization process. This is because our algorithm does not assume any knowledge about the original digitization process. Even so, if the number of background voxels converted into foreground ones is not too large, the input and output images will be similar, which is satisfactory for several applications that benefit from using well-composed images.

The conversion process relies on the fact that well composedness is a local property: that is, the condition of being well composed is equivalent to the nonexistence of two types of local critical configurations of image voxels[1] (see Figure 1). The first of these is where four voxels share an edge, two of them are background voxels, two of them are foreground voxels, and the background (or foreground) voxels share an edge but not a face. The second is where eight voxels share a vertex, two of them are background (or foreground), six of them are foreground (or background) voxels, and the two background (or foreground) voxels share a vertex but not an edge. It can be shown that a 3D binary digital image is well composed if, and only if, it does not contain any instances of these critical configurations.

Note that we can decide if a given 3D binary digital image is well composed by simply verifying if any 2×2×1 neighborhood of voxels of the image is an instance of the first critical configuration, and if any 2×2×2 neighborhood of voxels of the image is an instance of the second. This test can be performed in linear time with the number of voxels of the image. The first step of our algorithm is to verify if the input 3D binary digital image is well composed. If so, the algorithm finds a subset P of background voxels such that, if they were converted into foreground voxels, then the resulting image would be well composed. Then this conversion is performed.

Ideally, P should be as small as possible, so that the input and output images are similar. Although such a smallest set can be found using an exponential-time search, this is completely unfeasible in the context of practical applications. Our repairing algorithm is not guaranteed to find the smallest set P, but its time complexity is linear in the number of voxels of the input image. Our algorithm builds P iteratively, starting with an empty set. Each iteration inserts a background voxel into P. Each such voxel is randomly chosen from those in the background in the critical configurations of the input image, and when such a voxel is converted into a foreground one, at least one instance of a critical configuration is eliminated. This conversion can also give rise to a new critical configuration, which is further eliminated by choosing another background point. However, this process is guaranteed to converge to a correct solution after a finite number of iterations.

We tested our algorithm against several magnetic resonance (MR) images of parts of the human body, such as the brain, torso, and lungs. In all cases, our algorithm generated a well-composed image by converting fewer than 0.0034*N, where N is the total number of voxels in the input 3D binary digital image. We also derived an upper bound for the average number of voxels that needed to be converted. This upper bound supports the results obtained from our experiments with real imaging data, and provides a theoretical measure of the effectiveness of our algorithm for making 3D binary digital images well-composed. For future work, we intend to study the existence of a linear-time algorithm for computing the smallest subset of background voxels that generates a well composed image after being converted into foreground voxels.

Marcelo Siqueira, Longin Jan Latecki,* and Jean Gallier
Department of Computer and Information Science
University of Pennsylvania, Philadelphia, PA
*Department of Computer and Information Sciences
Temple University, Philadelphia, PA
E-mail: marcelos@seas.upenn.edu

References

1. L. Latecki, *3d well-composed pictures,* **Graphical Models and Image Processing 59** (3), pp. 164-172, 1997.
2. L. Latecki, U. Eckhardt, and A. Rosenfeld, *Well-composed sets,* **Computer Vision and Image Understanding 61** (10), pp. 70-83, 1995.
3. H. Dellingete, *Initialization of deformable models from 3d data,* **Proc. 6th Int'l Conf. in Computer Vision,** pp. 311-316, Bombay, India, 4-7 January 1998.
4. N. Krahnstoever and C. Lorenz, *Computing Curvature-Adaptive Surface Triangulations of Three-Dimensional Image Data,* **The Visual Computer 20,** pp. 17-36, 2004.
5. A. Gross and L. Latecki, *Digitizations preserving topological and differential geometric properties,* **Computer Vision and Image Understanding 62** (3), pp. 370-381, 1995.

Information processing of motion in facial expression and the geometry of dynamical systems

Amir H. Assadi, Brenton W. McMenamin, Department of Mathematics, University of Wisconsin; **Hamid R. Eghbalnia,** Department of Mathematics, Department of Biochemistry, University of Wisconsin

The advent of wireless communication has opened up a new era of multidisciplinary human and computer vision. Video conferencing now boasts transmission of realistic facial motion, albeit at a cost in terms of bandwidth and imperfect resolution. However, communicating the expression of a speaker's facial motion and the listeners' emotional response is a far more complex problem. The subtlety rests in the easy-to-experience fact that a drop in time-resolution causes the movement of facial features to be perceived as jerky, and that the viewers often cannot ignore a drop in spatial resolution. Time-variation of image frames stored in a video file can be regarded as a dynamical system realized through vector representation of images in sequences of frames in an Euclidean space of dimension D. How can we refine this naive representation to reduce the staggeringly high computational resources required to a practical range while retaining low error rates and other practical advantages?

Latecki *et al.*[1] have treated some of the more subtle points of digital geometry. The issue of when a discrete object obtained via the sampling of visual motion—as for the above-mentioned example of video—could be treated as a bona-fide geometric analogue of a curve. Further, the type of invariants associated with it are within the realm of digital geometry. An alternative, and still general, point of view is to regard a curve of this type as the flow line (an integral curve) of a dynamical system in a high-dimensional space. This works provided we resolve the delicate issues of reconciling perceptual and differential geometry (e.g. as discussed in Assadi *et al.*,[2] Eghbalnia *et al.*[3] and Townsend *et al.*.[4])

The exact encoding of realistic facial motions that convey emotions for a particular person **P** forms a parameter space $\mathbf{X}_\mathbf{P}$ that represents the *objective geometry* of the problem, the geometric features, and a representation of the space independent of evaluations by observers. The *subjective geometry* of $\mathbf{X}_\mathbf{P}$ varies between observers, reflecting individual experiences and variation in the perception of facial expressions. The encoding, compression, and communication of the subjective geometry of $\mathbf{X}_\mathbf{P}$ is the ultimate goal of an effective algorithm for transmitting this genre of multimedia.

The first problem is to find a way to encode the finer details of $\mathbf{X}_\mathbf{P}$ in real-time, and to select a sparse representation adaptively by the observer's feedback to the system. Psychophysical experiments are required to weigh the various features in $\mathbf{X}_\mathbf{P}$ according to the subjective valence of emotion for each individual: the design of such experiments poses an interesting problem in its own right. We recognize, then, that certain geometric invariants of digital geometry of the original motion data could be measured and singled out statistically. Each video frame is first encoded by an orthogonal decomposition (see Eghbalnia *et al.*[5]), thus encoding the motion in terms of significant coefficients of one such multi-scale decomposition.

Consider a discrete time-window W of length w sliding in the interval $\{a=t_0, b=t_{q-1}; t=t_0, t_1, \ldots t_{q-1}\}$, and the principal component analysis (PCA) of the data set $\mathfrak{D}_k(W)$ consisting of the frames of $\mathbf{X}_k(t)$ indexed by w. The window W provides two parameters τ (the starting point in time) and w, thus it also supplies the principal values and principal directions of $\mathfrak{D}_k(W)$ and other functions of the pair (τ, w). As in our earlier results in dynamic PCA for multi-channel time series[13], each scalar function of the principal values provide a function $F(\tau, w)$. Also, a vector whose components are $F_1(\tau, w)$, $F_2(\tau, w)$, …, $F_N(\tau, w)$ provides an *information surface* in $\mathbf{R}^N$. Every orthonormal frame of three top principal vectors provides a surface in the Stieffel manifold and the corresponding Grassmannian whose statistics are provided by a relatively small number of almost-constant clusters.

When the multi-channel time-series associated with $\mathfrak{D}_k(W_1)$, $\mathfrak{D}_k(W_2)$,… $\mathfrak{D}_k(W_r)$,… convey the same information-theoretic PCA output, their images under the mapping above are either the same or very close together. The images are either significantly far from each other, or could be assigned to distinct clusters in terms of the statistical analysis (such as the *principal frames* above.) Each cluster encodes features that carry essentially the same Shannon information relating to the multi-channel time series and $\mathfrak{D}_k(W)$, thus providing a class of algorithms for computing the sparse codes derived from the geometry of motion.

The statistical geometry of invariants of the parameters $\mathbf{X}_\mathbf{P}$ for a sample of population could provide effective algorithms for extraction of perceptually significant features in motion (e.g. in unsupervised feature detection from facial motion.) We have discussed problems of finding a sparse representation of motion features in circumstances such as normal conversations without discernible emotional expression or with perceptually-distinguishable emotional expression. We have also outlined a framework for study of their information-theoretic invariants. The algorithm provides a general approach to encode motion in terms of a particular genre of dynamical systems and the geometry of their flow (integral curves). In particular, a sparse coding of the video sequences is proposed that potentially classifies the features based on information-theoretic arguments. Examination of these sparse codes determines which ones reveal perceptually-significant events in motion, in distinction to those that fall into the category of frequent and common facial motions in an ordinary serious conversation.

Amir H. Assadi*, Hamid R. Eghbalnia*†, and Brenton W. McMenamin*
*Department of Mathematics
†Department of Biochemistry
University of Wisconsin, Madison, WI
E-mail: ahassadi@wisc.edu

References

1. L. J. Latecki, et al, **IEEE Advanced Video and Signal Based Surveillance,** 2003.
2. A. Assadi, S. Palmer, and G. Eghbalnia, **Proc. of IEEE NNSP '99,** Ed. T. Adali et al, 1999.
3. H. Eghbalnia, A. H. Assadi, and J. Townsend, Invited Chapter in **Handbook of Geometric Methods in Vision,** Ed. E. Bayro, Springer-Verlag, 2005.
4. J. Townsend, A. Assadi, and J. Busemeyer, Invited Chapter in **Measurement And Representation Of Sensations,** Eds. H. Colonius et al, Erbaum, Berlin, 2005.
5. H. Eghbalnia and A. H. Assadi, **J. Neurocomputing 40,** pp. 1155-1163, 2001.

Three-dimensional inspection

Continued from page 4.

Olivier Morel, Christophe Stolz, Fabrice Meriaudeau, and Patrick Gorria
Laboratory Le2i
Le Creusot, France
E-mail: o.morel@iutlecreusot.u-bourgogne.fr

References

1. S. Rahmann, *Reconstruction of quadrics from two polarization views*, **Proc. IbPRIA03 Iberian Conf. on Pattern Recognition and Image Analysis**, pp. 810-820, 2003.
2. D. Miyazaki, M. Kagesawa, and K. Ikeuchi, *Transparent surface modeling from a pair of polarization images*, **IEEE Trans. Pattern Anal. Machine Intell. 26** (1), pp. 73-82, 2004.
3. L.B. Wolff, and T.E. Boult, *Constraining object features using a polarization reflectance model*, **IEEE Trans. Pattern Anal. Machine Intell. 13** (7), pp. 635-657, 1991.
4. O. Morel, C. Stolz, and P. Gorria, *Application of Polarimetric Imaging to 3D Inspection of Highly Reflective Metallic Surfaces*, **Proc. SPIE 5606,** pp. 82-89, 2004.

Digital bullet scratches

Jan Lukas, Jessica Fridrich, and Miroslav Goljan, Department of Electrical and Computer Engineering, SUNY Binghamton

Is it possible to use the fine structure of pixel colors in an image to identify the digital camera that took it, in much the same way that we can identify a gun by looking at the scratches it made on the bullets it fired? If so, how reliably can we distinguish between images obtained using different sensors or cameras? Is accurate identification possible even from processed images? Reliable digital-camera identification would especially prove useful in court for establishing the origin of images presented as evidence, or, in a child-pornography case, to prove that certain imagery was obtained using a specific camera and is not computer-generated.

In classical film photography, there are methods for camera identification that are commonly used in forensic science. Some of these methods use camera imperfections, such as scratches on the negative caused by the film transport mechanism. To find an appropriate equivalent for the digital realm, one needs to turn to the process of digital data acquisition.

In a typical consumer digital camera, the light from the photographed scene passes through the camera lenses. However, before reaching a photo responsive sensor, the light goes through an antialiasing (blurring) filter and then through a color filter array (CFA). The photon counts are converted to voltages, which are subsequently quantized by an analog-to-digital converter. The digital signal is then interpolated (demosaicked) using color interpolation algorithms, color corrected, and the white balance adjusted. Additional processing includes high-pass filtering and gamma correction to adjust for the linear response of the imaging sensor. Finally, the raw image is written to the camera memory device in a user-selected image format (e.g., TIFF or JPEG).

Basing camera identification on artifacts introduced by CFA or processing would not permit us to distinguish between cameras that share the same sensors or processing algorithms. Thus, to obtain a unique identification fingerprint, we need to turn our focus to the imaging sensor, which is usually a CCD (charge-coupled device) or a CMOS (complementary metal oxide semiconductor) array.[1] Imperfections of different kinds are introduced into each sensor during the manufacturing process. As these imperfections are of a stochastic nature and are unlikely to be identical for different sensors, they can be used to identify the camera in a manner similar to identifying people by their birthmark. Among the most commonly present defects are hot and dead pixels. The problem with these is that some cameras remove them from images by post-processing and some cameras may not have any of these defects.

Instead of relying on defective pixels,[2] we have proposed a new approach that uses the pattern noise of CCD arrays.[3] This is, in fact, a collection of patterns caused by different phenomena, such as pixel-to-pixel non-uniformity, dust specs on optics, interference in optical elements, and dark current. However, not all of them are suitable for our goal. We are interested in those noise components that do not change with time, at least in the short term, and that allow reliable extraction from typical images. These requirements are best satisfied for pixel-to-pixel non-uniformity, which is caused by slight differences in the efficiency with which individual pixels absorb photons. The differences are stochastic in nature and are inevitably caused during the manufacturing process. As a result, each image the camera takes is overlaid with a weak noise-like pattern.

We extract this pattern using a denoising filter. To minimize the impact of the scene and improve the estimation process, we average these patterns extracted from many images taken with the same camera, thus obtaining the camera 'reference pattern'. To determine whether a specific image was taken with this camera, we simply extract the noise pattern from the image and calculate its correlation with the camera reference pattern. Based on the correlation value, we can reach a decision about the image origin.

This methodology was tested on nine different devices: low-end digital cameras; two semi-professional DSLRs (Nikon D100 and Sigma SD9); and the camera containing the Foveon X3 CMOS sensor (Sigma SD9). Our set also contained two cameras of exactly the same make (two Olympus Camedia C765 UZ).

The task that one typically encounters in practice is to determine from several cameras the camera that most-likely took a given image. This can be achieved simply by assigning the image to the camera whose reference pattern has the highest correlation with the noise from the image. In our experiments with nine cameras and a total of 3000 images in both raw and JPEG formats, all images were correctly classified. We were also able to correctly identify the camera from images that were processed using lossy JPEG compression with quality factors as low as 72 and additionally resized with an adjusted contrast. Our experiments also confirmed that it is possible to distinguish between cameras of the exact same model.

Jan Lukas, Jessica Fridrich, and Miroslav Goljan
Department of Electrical and Computer Engineering
SUNY Binghamton, NY
E-mail: {jan.lukas, fridrich, mgoljan}@binghamton.edu

References

1. G. C. Holst, **CCD Arrays, Cameras, and Displays,** 2nd edition, JCD Publishing and SPIE Press, USA, 1998.
2. Z. Geradts, J. Bijhold, M. Kieft, K. Kurosawa, K. Kuroki, and N. Saitoh, *Methods for identification of images acquired with digital cameras,* **Proc. SPIE 4232,** pp. 505-512, 2001.
3. J. Lukas, J. Fridrich, and M. Goljan, *Determining digital image origin using sensor imperfections,* **Proc. SPIE 5685,** 2005.

Machine vision for defect detection

Continued from page 3.

References

1. C. E. Thomas Jr., et al. *Direct to digital holography for high aspect ratio inspection of semiconductor wafers,* **2003 Int'l Conf. on Characterization and Metrology for ULSI Technology, Proc. AIP Vol. 683**, pp. 254-270, Austin, March 2003.
2. P. Bourgeat, F. Meriaudeau, P. Gorria, and K. W. Tobin, *Content-based segmentation of patterned wafer for automatic threshold determination,* **Proc. SPIE 5011,** pp. 183-189, 2003.
3. P. Bourgeat, F. Meriaudeau, K. W. Tobin, and P. Gorria, *Patterned wafer segmentation,* **Quality Control by Artificial Vision, Proc. SPIE 5132**, pp. 36-44, 2003.
4. P. Bourgeat, **Segmentation d'images de semi-conducteurs appliquée à la détection de défauts,** Ph.D. thesis, Université de Bourgogne, 2004.
5. P. Bourgeat, F. Meriaudeau, K. W. Tobin, and P. Gorria, *Features extraction on Complex images,* **Proc. OSAV'2004, Int'l. Topical Meeting on Optical Sensing and Artificial Vision**, pp. 103-110, Saint Petersburg, Russia, 18-21 October 2004.
6. F. Meriaudeau, P. Bourgeat, P. Gorria, and K. Tobin, *Classifier Combination on Features extracted From Complex images: Application to Defect Detection on Silicon Wafers,* **Proc. QCAV'05**, Japan, May 2005.

Motion-based particle filtering for head tracking applications

Nidhal Bouaynaya and Dan Schonfeld, Multimedia Communications Laboratory, University of Illinois

Recent advances in multimedia and communication require techniques for accurately tracking objects in video sequences. The goal in tracking is to estimate the posterior density of the target given all the observations. The estimate of the object is then given by the mean state estimate. Particle filters provide a general framework for estimating the probability-density function of general non-linear and non-Gaussian systems.

Let X_k represent the target characteristics at discrete time k (position, velocity, shape, etc). Denote all past observations up to time k by $\mathbf{Z}_{1:k} = \{z_0,\ldots,z_k\}$. Given a Markovian state space model for X_k, we want to estimate the posterior density $p(X_k \mid \mathbf{Z}_{1:k})$. Let $\{X_k^{(n)}, \text{n=1},\ldots,\text{N}\}$ be a set of samples drawn from a distribution q at time k. Let the set of weights $\{\pi_k^{(n)},\text{n=1}\ldots\text{N}\}$ be given by:

$$\pi_k^{(n)} = \pi_{k-1}^{(n)} \frac{p(X_k^{(n)} \mid X_{k-1}^{(n)})}{q(X_k^{(n)})} p(Z_k \mid X_k^{(n)})$$

Then, it can be shown that the posterior density is approximated, at time k, by the weighted sample $\{ (X_k^{(n)}, \pi_k^{(n)}), \text{n=l},\ldots,\text{N} \}$.[1] The conditional densities $p(X_k \mid X_{k-1})$ and $p(Z_k \mid X_k)$ are specified by the state space model. Notice that, in theory, there is infinite number of choices of the importance function q, as long as its support includes that of the posterior distribution. But of course when q is close to the true posterior, the particles are more effective.

We propose a motion-based proposal. We adopt adaptive block matching (ABM) as the motion-estimation technique.[2] We use a four-dimensional parametric ellipse to represent the state vector of the head. The motion vector of interest, ΔX_k, is given by the difference between the position of the center of the newly-fitted ellipse and the position of the center of the previous mean-state ellipse.

Each sample is translated in the *x-y* direction by the motion vector estimated by the ABM and diffused in the four coordinates according to a zero-mean white Gaussian noise. The motion-based importance function is then a sum of Gaussians:

$$g(X_k) = \frac{1}{N}\sum_{n=1}^{N} \mathcal{N}(X_{k-1}^{(n)} + \Delta X_k, \Sigma),$$

where the notation $N(\mu, \Sigma)$ denotes the normal distribution with mean μ and covariance matrix Σ.

In addition to the importance-function evaluation, we also need to calculate the particle likelihood $p(Z_k \mid X_k)$ and transition probability $p(X_k \mid X_{k-1})$.

We use both face-color characteristics and edge-detection cues for the likelihood term. We use the color model proposed in Reference 3 and the gradient model described in Reference 4. We adopt a first order auto-regressive (AR1) process for the system dynamics.

Refinement process

Applications, such as interactive imaging or virtual reality environments, need an accurate elastic contour around the person's head. Active contours take an initial estimate of the object and refine this estimate using an optimization procedure.

We simplify the 2D contour into a 1D model by considering only observations $\lambda\phi$ along the normal lines σ of the contour. The total energy is a weighted sum of different energy terms. The weights are fixed for the whole video. The different energy terms are defined as follows:

$E_{ext}(\lambda_\phi) = -|I(\lambda_\phi + 1) - I(\lambda_\phi)|^2$ is the external force making the contour move towards the edges, where I denotes the intensity.

$E_{\text{int}}(\lambda_\phi, \lambda_{\phi-1}) = |\lambda_\phi - \lambda_{\phi-1}|^2$ is the internal energy term and imposes smoothness on the contour.

$E_{shape}(\lambda_\phi) = \frac{\lambda_\phi^2}{\sigma^2}$ is the shape energy term,

where σ specifies the accuracy of the initial contour.

The causal definition of all the energy terms allows a dynamic programming scheme to find the optimal sequence. To improve the performance of the active contour, we perform the optimization procedure using properly-sampled initial conditions. Specifically, we draw normally-distributed samples with the mean of the initial output of the tracker and a given covariance. Dynamic programming is performed for each sample. The optimal elastic contour is then the one that corresponds to the minimum total energy.

Experiments

Our experiments applied this technique to head tracking. We use challenging video sequences with more than 400 frames in cluttered environments. We simulate various tracking conditions, including camera zoom in and out, appearance changes, fast and erratic movements, out-of-plane head rotation. During the tracking, 50 particles are propagated. The refinement stage uses 10 perturbed initial samples.

Conclusions

In this paper, we have demonstrated that real-time information extraction can be incorporated into the importance density function of particle filters to significantly improve the tracking performance. Specifically, we showed that online motion estimation can be used to track fast-moving objects that undergo erratic movements. Moreover, the use of a robust contour extraction scheme allows us to employ the proposed tracking system in many applications (e.g., background hiding, virtual video-conferencing, video animation, robust processing, etc.).

Nidhal Bouaynaya and Dan Schonfeld
Multimedia Communications Laboratory
Department of Electrical and Computer Engineering
Univ. of Illinois, Chicago, IL
E-mail: {nbouay1,dans}@uic.edu.

References

1. A. Doucet, *On sequential simulation-based methods for bayesian filtering,* **Technical report CUED/F-INFENG/TR.310,** 1998.
2. K. Hariharakrishnan and D. Schonfeld, *Fast object tracking using adaptive block matching,* **IEEE Trans. on Multimedia,** *to appear.*
3. K. Nummiaro, E. Koller-Meier, and L. V. Gool, *Object tracking with an adaptive color-based particle filter,* **DAGM-Symp. Pattern Recognition,** pp. 353-360, 2002.
4. M. Isard and A. Blake, *Condensation conditional density propagation for visual tracking,* **Int. J. Computer Vision 29,** pp. 528, 1998.

Figure 1. Motion-based particle filter handles fast motion and out-of-plane rotation of the jumping person simultaneously .

Figure 2. Randomly-perturbed active contour results. The elastic contour nicely fits the head, which can then be easily extracted for further processes.

Managing levels of detail for real-time rendering in immersive virtual environments

D. Paillot, F. Mérienne, M. Neveu, and S. Thivent, Le2i laboratory, Institut Image

Design reviews in virtual immersive environments for the motor industry need a very-high geometrical quality, and real-time visualization and interactivity. To be useful, such applications have to be linked to the relevant computer-aided design (CAD) database. At the same time, to work with virtual-reality applications, CAD models have to be prepared in advance as digital mock-ups (DMUs). Currently, it takes several months to get a full car model into a virtual reality application. In this article, a complete chain for exporting CAD designs into virtual reality models is proposed and developed (see Figure 1).

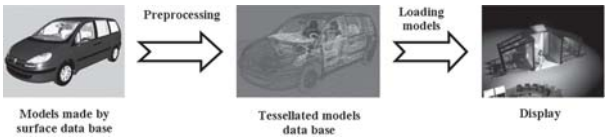

Figure 1. The steps for exporting CAD models into virtual-reality models.

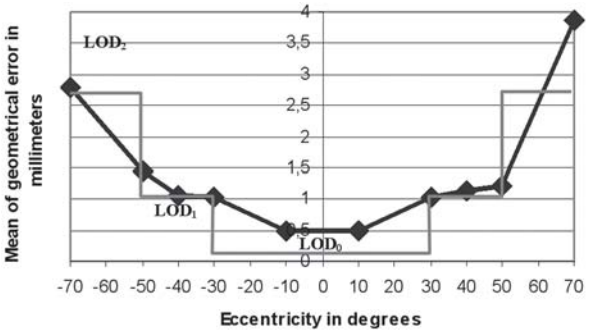

Figure 2. Geometrical-error dependency on the eccentricity.

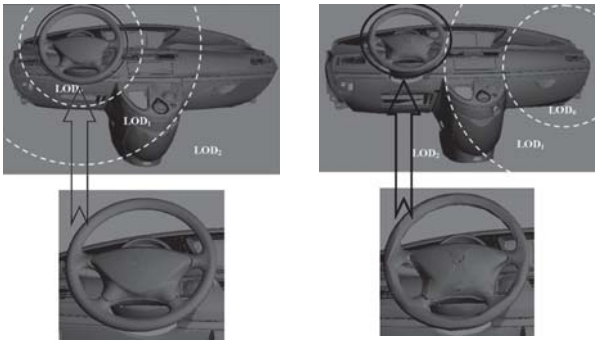

Figure 3. Rendering scheme for two viewing directions: (a) looking at the wheel; (b) looking on the right side on the dashboard.

Preprocessing

Since CAD models cannot be used in real time, data preparation is required. This step is composed of three stages: the tessellation that converts a model made by surfaces into a set of polygons; the repair of the polygons (deletion of multiple entities, welding vertices/edges, etc.); and the deletion of all invisible parts of the assembly (rib, rivets, screw holes, etc.). We implement this stage using the P-Buffer algorithm, which requires as parameters the directions of visualization represented by different points of view of the assembly. For example, in the proposed implementation, the reduction ratio for a dashboard is typically about 75%. All these stages optimize the models for the best visual quality. The digital mock-up operations must be as precise as the physical mock-up.

For the design review of the interior of the vehicle, all objects that are rendered using the virtual models are viewed in a cave-like environment: everything is approximately the same distance from the observer and is distributed 360° around. In practice, due to the requirements of real-time processing, a special scheme is needed to reduce the elements needed for rendering. This is referred to as level-of-detail (LOD) management.[1] Previously-published techniques, known as decimation,[2] can be used. Our reduction scheme offers the best trade off between the perceived quality of rendering and the number of polygons required for scene rendering, based on the response of the human visual system in this environment.

Loading models

The proposed method involves displaying a model with a controlled definition depending on the visual acuity of the observer. Visual acuity is a function of the eccentricity of the retina and can be evaluated by showing two models with various LOD at different eccentricities. The viewer is asked to distinguish between them. An equal perception of two different models means that the human visual system has reached its limit. A statistical analysis allows us to define the geometrical error limit depending on the eccentricity. Results are presented on the Figure 2 (black curve). This result is similar to the curve proposed by M. Reddy,[3] which represents the visual acuity depending on the eccentricity.

This perception limit can be used for LOD management. The viewing direction is indicated in real time by a head-tracking system, so the eccentricity for each model into the scene can be adjusted. Using the dark curve in the Figure 2, a decimated model can replace the reference without decreasing the perception quality. To limit the computational time, three LOD schemes are chosen, corresponding to the grey line in the Figure 2.

Results

Experiments were performed on a dashboard of the 807-C8 car from PSA Peugeot-Citroen Company: there were 54 objects in total. Each was decimated with three geometrical errors (0.25mm, 1mm, and 2.75mm). When all the models were displayed without decimation, the frame rate was 7fps for 500,000 polygons. With the LOD management depending on the eccentricity, the frame rate and the number of polygons in the scene change in real time. Figure 3 illustrates the rendering for two viewing directions: (a) looking at the wheel; and (b) and looking on the right side of the dashboard. The limits of the LOD zone are marked in white. The proposed scheme reduces the number of polygons to 94,000, thus increasing the frame rate to about 23fps without a decrease in the observed visual quality of rendering.

D. Paillot, F. Mérienne, M. Neveu, and S. Thivent
Le2i laboratory
Institut Image
Chalon sur SaÙne, France
E-mail: paillot@cluny.ensam.fr

References

1. J. H Clark, *Geometric Models for Visible Surface Algorithm,* **Communication of the ACM 19** (10), pp. 547-554, 1976.
2. P. Heckert and M. Garland, *Multiresolution modelling for fast rendering,* **Proc. of Graphics Interface '94,** pp. 43-50, 1994.
3. M. Reddy, **Perceptually Modulated Level Of Detail for Virtual environment,** Ph.D. Thesis (CST-134-97), University of Edinburgh, 1997.

Imaging arithmetic: Physics ∪ Math > Physics + Math

Continued from cover.

mation from the back-side printing can often be seen in the resulting images (of the front side of the page). This show-through is normally an undesirable artifact in the scan that one would like to remove. An example of show-through can be seen in Figure 1, where the scanned images from two sides of a duplex printed page are shown with visible show-through in both.

Traditionally, thresholding is used to minimize the effect of show-through. Thresholding sets scanned reflectance values above a selected threshold to unity (white). This approach works well for pure black and white regions (e.g. Figure 1(a)), but fails irretrievably for show-through seen in a light gray background, for instance, in the region corresponding to the state of Texas in Figure 1(b).

When scans of both sides of the page are available, the problem of show-through removal becomes analogous to the signal processing problem of echo cancellation.[2] The images of the two sides help distinguish light gray printing on the front side from show-through due to the back side. This by itself is, however, insufficient for the development of a method for correction because the show-through is a non-linear and image-dependent effect in the image intensity domain (note that dark regions on the front side have no impact of show-through). A physical understanding of the show-through process is required in order to proceed. An elementary physical model can be developed by considering the optical properties of the elements involved. Through suitable simplification using the fact that the paper substrate scatters (or reflects) back a much larger fraction of the incident light than it transmits, it is possible to obtain a linearized model for show-through of the form:[3]

$$D_f^s(x,y) \approx D_f(x,y) + h(x,y) \otimes A_b^s(x,y) \quad (1)$$

where (x,y) denotes spatial location, $D_f^s(x,y)$ is the (optical) density of the front side scan (defined as the negative logarithm of the scan reflectance normalized by the white paper reflectance), $D_f(x,y)$ is the density that would have been obtained in the absence of any printing on the front side, $h(x,y)$ is the 'show-through point spread function', $\otimes$ represents the convolution operator, and $A_b(x,y)$ is the absorptance of the back side (defined as one minus the back-side scan reflectance divided by the paper reflectance). The show-thorough point spread function (PSF) represents physical model terms that ensure its value is small in spatial extent similar to a blurring filter.

Note that the equation is rather non-intuitive, in that two of the terms are in density and a third in absorptance. *The equation would be rather hard to arrive at purely through trial and error with different mathematical transforms. It, however, comes about naturally from the physical model of the problem with the use of the appropriate mathematical simplification.*

Once the linearized model of show-through is available, the mathematical signal-processing technique of adaptive filtering can be applied to the problem of show-through correction. This technique has the useful capabilityof automatically estimating and tracking the show-through PSFs $h(x,y)$ are caused both by changes in paper substrate and variations in registration between the front and back-side images due to imperfections in the scanning process. We present only sample results here and refer the interested reader to Reference 3 for additional details.

Corrected images (see Figure 2) corresponding to the scans of the two sides shown in Figure 1 were obtained using the show-through cancellation algorithm. From the results, it is clear that the algorithm is successful. It is effective in eliminating the show-through not only in white regions of the page but also in light gray regions, such as those corresponding to the state of Texas in these figures.

Discussion and summary

The example presented here illustrates how the problem of show-through in document imaging can be solved by using suitable physical models and mathematical tools. It is worth pointing out that the synergy and combination of these elements is what allows the solution: either one by itself is insufficient. The use of gradient-descent-based adaptive filtering by itself does not enable the solution. Instead, the physical analysis that allows linearization of the problem is also a key element. In particular, the problem becomes linear when image data on the front side is converted to density and on the back side to absorptance: a rather non-intuitive result that could be inferred only through the use of the physical model. Likewise, the physical modeling by itself is rather simplistic and is not sufficient to solve the problem since it does not readily allow us to compute the unknown show-through point-spread function or the alignment between the images on the two sides.

The synergy between physics and mathematics is a particularly common and powerful motif in imaging systems research that is supported by numerous other examples. The interdisciplinary nature of work in imaging systems makes these approaches that combine physics and mathematics harmoniously even more compelling than other areas of research.

Gaurav Sharma
Electrical and Computer Engineering and
Biostatistics & Computational Biology Depts.
University of Rochester, NY
E-mail: gsharma@ece.rochester.edu

References

1. G. Sharma, *Imaging Arithmetic: Physics ∪ Math > Physics + Math,* **Proc. SPIE 5667,** pp. 95-106, Invited Paper, 2005.
2. S. Haykin, **Adaptive Filter Theory,** Prentice Hall, NJ, 2002.
3. G. Sharma, *Show-through cancellation in scans of duplex printed documents,* **IEEE Trans. Image Proc., 10** (5), pp. 736-754, May 2001.

Deflectometric inspection of diffuse surfaces

Continued from page 12.

movement is assumed. For this scenario, the pattern is fixed. The necessary phase shift of the pattern is achieved by the movement of the work-piece on the assembly line. As a periodic fringe pattern is used, one can automatically calculate the actual phase shift of the pattern. This is done by calculating the pixel-wise contrast between two particular images: the first image, with phase shift zero; and a second image, the relative phase shift of which has to be determined. The pixel-wise contrast between these images is averaged over the whole image region. Maximum contrast is reached for a 180° phase shift, minimum contrast for 360°. With this knowledge, four images with 90° phase shift can be selected from the image sequence acquired at the assembly line. Deflectometry in general is very successful for the inspection of specular surfaces. Using our new far-infrared extension of the technique, plastics and beamless metal sheets can be inspected. For example, a high-quality examination of car body parts can now be carried out prior to the costly varnishing.

Jan W. Horbach and Soeren Kammel
Institute for Measurement and Control Systems
University of Karlsruhe, Germany
E-mail: {horbach, kammel}@mrt.uka.de

Join the SPIE/IS&T Technical Group

...and receive this newsletter

This newsletter is produced twice yearly and is available only as a benefit of membership of the SPIE/IS&T Electronic Imaging Technical Group.

IS&T—The Society for Imaging Science and Technology has joined with SPIE to form a technical group structure that provides a worldwide communication network and is advantageous to both memberships.

Join the Electronic Imaging Technical Group for US$30. Technical Group members receive these benefits:

- *Electronic Imaging* Newsletter
- SPIE's monthly publication, ***oe****magazine*
- annual list of Electronic Imaging Technical Group members

People who are already members of IS&T or SPIE are invited to join the Electronic Imaging Technical Group for the reduced member fee of US$15.

Please Print ☐ Prof. ☐ Dr. ☐ Mr. ☐ Miss ☐ Mrs. ☐ Ms.

First (Given) Name _____ Middle Initial _____

Last (Family) Name _____

Position _____

Business Affiliation _____

Dept./Bldg./Mail Stop/etc. _____

Street Address or P.O. Box _____

City _____ State or Province _____

Zip or Postal Code _____ Country _____

Phone _____ Fax _____

E-mail _____

Technical Group Membership fee is $30/year, or $15/year for full SPIE and IS&T Members.

Amount enclosed for Technical Group membership **$** _____

❑ **I also want to subscribe to IS&T/SPIE's *Journal of Electronic Imaging* (JEI)** **$** _____
(see prices below)

Total $ _____

❑ **Check enclosed.** Payment in U.S. dollars (by draft on a U.S. bank, or international money order) is required. Do not send currency. Transfers from banks must include a copy of the transfer order.

❑ **Charge to my:** ❑ **VISA** ❑ **MasterCard** ❑ **American Express** ❑ **Diners Club** ❑ **Discover**

Account # _____ Expiration date _____

Signature _____
(required for credit card orders)

Reference Code: 4646

JEI 2005 subscription rates (4 issues):	**U.S.**	**Non-U.S.**
Individual SPIE or IS&T member*	$ 55	$ 55
Individual nonmember and institutions	$305	$330

Your subscription begins with the first issue of the year. Subscriptions are entered on a calendar-year basis. Orders received after 1 September 2005 will begin January 2006 unless a 2005 subscription is specified.

One online journal included with SPIE/IS&T membership. Price is for printed journals.

Send this form (or photocopy) to:
SPIE • P.O. Box 10
Bellingham, WA 98227-0010 USA
Tel: +1 360 676 3290
Fax: +1 360 647 1445
E-mail: membership@spie.org

Please send me:
☐ **Information about full SPIE membership**
☐ **Information about full IS&T membership**
☐ **Information about other SPIE technical groups**
☐ **FREE technical publications catalog**

Electronic Imaging

The *Electronic Imaging* newsletter is published by SPIE—The International Society for Optical Engineering, and IS&T—The Society for Imaging Science and Technology. The newsletter is the official publication of the International Technical Group on Electronic Imaging.

Editor/Technical Group Chair	Gabriel Marcu
Technical Editor	Sunny Bains
Editorial Assistant	Stuart Barr
Managing Editor/Graphics	Linda DeLano

Articles in this newsletter do not necessarily constitute endorsement or the opinions of the editors, SPIE, or IS&T. Advertising and copy are subject to acceptance by the editors.

SPIE is an international technical society dedicated to advancing engineering, scientific, and commercial applications of optical, photonic, imaging, electronic, and optoelectronic technologies.

IS&T is an international nonprofit society whose goal is to keep members aware of the latest scientific and technological developments in the fields of imaging through conferences, journals and other publications.

SPIE—The International Society for Optical Engineering, P.O. Box 10, Bellingham, WA 98227-0010 USA. Tel: +1 360 676 3290. Fax: +1 360 647 1445. E-mail: spie@spie.org.

IS&T—The Society for Imaging Science and Technology, 7003 Kilworth Lane, Springfield, VA 22151 USA. Tel: +1 703 642 9090. Fax: +1 703 642 9094.

EIONLINE

Electronic Imaging Web Discussion Forum

You are invited to participate in SPIE's online discussion forum on Electronic Imaging. To post a message, log in to create a user account. For options see **"subscribe to this forum."**

You'll find our forums well designed and easy to use, with many helpful features such as automated email notifications, easy-to-follow 'threads,' and searchability. There is a full FAQ for more details on how to use the forums.

Main link to the new Electronic Imaging forum:

http://spie.org/app/forums/tech/

Related questions or suggestions can be sent to **forums@spie.org.**

The International Society for Optical Engineering

Deflectometric inspection of diffuse surfaces in the far-infrared spectrum

Jan W. Horbach and Soeren Kammel, Institute for Measurement and Control Systems, University of Karlsruhe

Deflectometry is an optical method for the inspection of specular freeform surfaces such as varnished car-body parts. Bumps, dents, waviness, scratches and coating defects can be detected using this method. Up to now, deflectometry was restricted to specular surfaces. The specular reflection from known patterns was analyzed, as the shape of the surface causes distortions in the pattern that provide information about the local surface curvature. Clearly, it would be advantageous to accomplish such an inspection prior to the costly varnishing process.

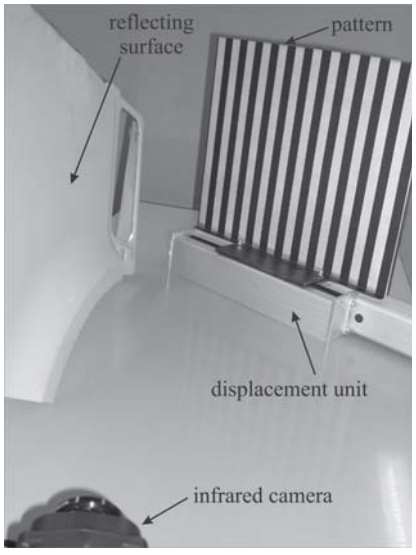

Figure 1. Setup for infrared deflectometry: infrared radiation is emitted as a pattern that is laterally shifted. The radiation is reflected from the part and observed by the infrared camera.

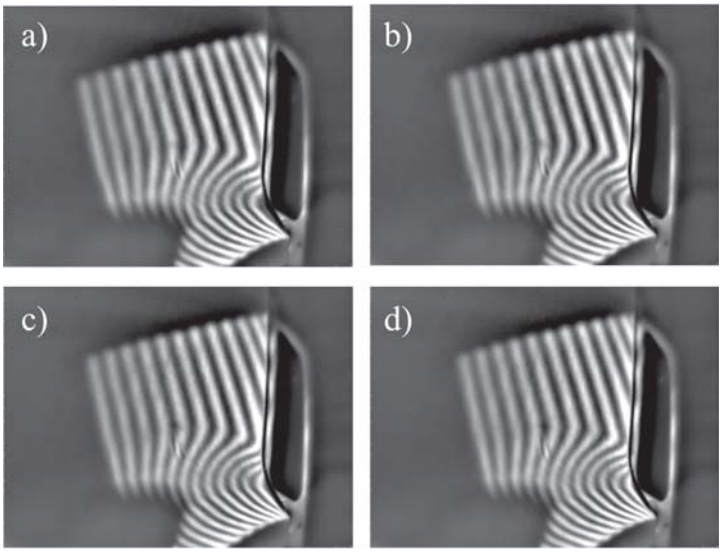

Figure 2. Four images of the reflected phase-shifted pattern. The phase shift is 90° between consecutive images, used to calculate the result.

This is now possible, using infrared technology. Even beamless objects like unpainted moulded or stamped parts are specular for far-infrared radiation. We developed a pattern generator that emits such radiation (see Figure 1), the reflection of which is observed using a thermal camera. We can realize a phase shift by performing a lateral movement of the pattern. By analyzing four images of the reflected phase-shifted pattern (see Figure 2) our algorithm can calculate the local curvature of the inspected object. It uses the fact that the curvature of a spherical mirror affects the focal point of the optical mapping. As the fringe pattern is shifted, each point on the surface is illuminated with changing brightness. The contrast between shifted images at the same point is influenced directly by the sharpness of the mapping and therefore by the local curvature of the reflecting point. This contrast information is visualized in the resulting image (see Figure 3).

In the example shown, a bump has been detected. As the part has not been painted yet, a human observer cannot see this defect. However, since the defect would become visible after painting, the part must be rejected. To get a sense of the overall performance of our system, we compared our results to that of tactile measurements. These tests showed that, using our setup, infrared deflectometry is able to detect bumps down to a minimum height of 15μm given a lateral dimension of the bump of about 2mm. Because our method is sensitive to local curvature, even flatter defects can be detected, if their lateral dimension becomes smaller.

We have shown that our method can be applied to a moving assembly line if constant

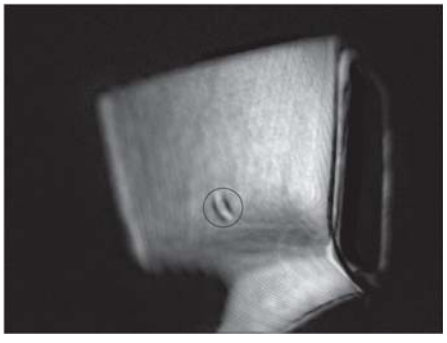

Figure 3. Resulting image: the local curvature of the surface is represented by the grey value. The detected bump is marked with a circle.

Continued on page 10.

SPIE Society of Photo-Optical Instrumentation Engineers
P.O. Box 10 • Bellingham, WA 98227-0010 USA

Change Service Requested
DATED MATERIAL

Non-Profit Org.
U.S. Postage Paid
Society of
Photo-Optical
Instrumentation
Engineers